

Journal of Geophysical Research: Atmospheres

RESEARCH ARTICLE

10.1002/2017JD027205

Key Points:

- An improved quasi-stochastic (IQS) model that allows for multiple collisions of cloud particles is evaluated through a case study
- Surface precipitation amount is larger in the IQS model than in the normal QS model, particularly over strong precipitation region
- Increased mass contents of both large and small drops in the IQS model together contribute to the larger surface precipitation amount

Correspondence to:J.-J. Baik,
jjbaik@snu.ac.kr**Citation:**

Lkhamjav, J., Jeon, Y.-L., Lee, H., Baik, J.-J., & Seo, J. M. (2017). Evaluation of an improved quasi-stochastic collection model through precipitation prediction over north central Mongolia. *Journal of Geophysical Research: Atmospheres*, 122, 13,404–13,419. <https://doi.org/10.1002/2017JD027205>

Received 26 MAY 2017

Accepted 4 DEC 2017

Accepted article online 12 DEC 2017

Published online 27 DEC 2017

Evaluation of an Improved Quasi-stochastic Collection Model Through Precipitation Prediction Over North Central Mongolia

Jambajamts Lkhamjav¹, Ye-Lim Jeon¹ , Hyunho Lee¹ , Jong-Jin Baik¹ , and Jaemyeong Mango Seo¹ 

¹School of Earth and Environmental Sciences, Seoul National University, Seoul, South Korea

Abstract One of the key components of bin microphysics schemes is the quasi-stochastic collection equation that describes the collection process of cloud particles. The normal quasi-stochastic model, hereafter the NQS model, assumes that the time step is infinitesimally small, so that a cloud particle can collide with other cloud particle only once within the time step. However, since the time step is finite, a cloud particle can collide with other cloud particle more than one time within the time step. Hence, the improved quasi-stochastic model that realizes this approach, hereafter the IQS model, is physically more reasonable. This study provides the evaluation of the IQS model against the NQS model in precipitation prediction. For this, a precipitation event observed over north central Mongolia on 21 August 2014 is simulated using the Weather Research and Forecasting model with a detailed bin microphysics scheme. The surface precipitation amount is larger in the IQS model than in the NQS model, particularly over the strong precipitation region. The IQS model increases the mass contents of small drops and large drops due to multiple collisions. The increased large drops contribute to the increase in surface precipitation amount. The increased small drops are transported upward, which eventually leads to an increase in snow mass content. Deposition and riming in the IQS model occur more actively, further increasing snow mass content. The increased snow mass content also contributes to the increase in surface precipitation amount through melting.

1. Introduction

Numerical models that resolve cloud and precipitation processes explicitly on grid scale have been increasingly used to better understand moist convection and accurately predict precipitation. They are categorized into numerical models that include bulk microphysics schemes, hereafter called bulk models, and numerical models that include bin microphysics schemes, hereafter called bin models (Houze, 2014; Khain et al., 2015). Bulk and bin models share common characteristics. For example, both the models usually classify hydrometeors into similar types (e.g., drops, cloud ice/crystals, snow, and graupel). However, bulk and bin models adopt fundamentally different approaches in the way they treat cloud microphysical processes, particularly in describing the size distribution of hydrometeors. In bulk models, the size distribution of precipitation particles is assumed to have a specific form (e.g., Marshall-Palmer distribution or gamma distribution). One-moment bulk models predict the mixing ratios of hydrometeors (e.g., Kessler, 1969; Lin et al., 1983), and two-moment bulk models predict the mixing ratios and number concentrations of hydrometeors (e.g., Lim & Hong, 2010; Seifert & Beheng, 2006). On the other hand, in bin models, the entire mass range of each hydrometeor is divided into discrete mass bins and the number concentration of each hydrometeor in each bin is predicted (e.g., Iguchi et al., 2012; Khain et al., 1996; Lynn et al., 2005a).

Bin models require much more computing times but represent microphysical processes more reliably than bulk models (Khain et al., 2015; Sato et al., 2009). Most numerical models and all the operational weather forecasting models have adopted bulk microphysics schemes. Recently, however, many studies have been performed to simulate moist convection and weather using bin models. Lynn et al. (2005a, 2005b) showed that the bin model simulates the rate and distribution of precipitation caused by mesoscale convection better than the bulk model. Iguchi et al. (2012) simulated a real case of shallow convective clouds and precipitation behind a cold front and obtained results from the bin model that are closer to the observation than those from the one-moment bulk model.

Many microphysical processes such as nucleation, vapor diffusion, freezing, melting, collision, breakup, and sedimentation are included in bin microphysics schemes. Among them, the collision process plays a key

role in the growth of cloud particles (Pruppacher & Klett, 1997). To describe the collisional growth of cloud particles, a quasi-stochastic collection equation that considers the stochastic concept (Berry, 1967; Telford, 1955) is utilized. Traditional quasi-stochastic models assume that the time step is infinitesimally small, so that a cloud particle can collide with other cloud particle only once within the time step and the average number of collisions is interpreted as a collision probability (Gillespie, 1972). However, since the time step used is finite, a cloud particle can collide with other cloud particle more than one time within the time step. By taking account of this, the probability distribution of the number of collisions within a time step can be expressed as a Poisson distribution (Lkhamjav et al., 2017; Young, 1975). Lkhamjav et al. (2017) simulated an idealized two-dimensional warm cloud using the improved quasi-stochastic (IQS) model and demonstrated that the onset of surface precipitation is accelerated as much as several minutes due to multiple collisions of cloud particles within a time step compared to the normal quasi-stochastic (NQS) model. As a next research step, it would be meaningful to examine differences in surface precipitation when the IQS and NQS models are compared through real-case prediction and find reasons for the differences. A small change in cloud microphysics in a three-dimensional model with full physics can sometimes result in large or noticeable changes in surface precipitation through complex nonlinear interactions between cloud microphysics and dynamics.

This study aims to evaluate the IQS model against the NQS model in precipitation prediction. For this, a numerical model coupled with an updated bin microphysics scheme is used to simulate a precipitation event observed over north central Mongolia. In section 2, the observational analysis for this precipitation event is given and the numerical model and the experimental setup are described. In section 3, the model is validated and the results from the IQS and NQS models are presented and discussed, particularly focusing on the impacts of the improvement in the quasi-stochastic model on clouds and precipitation. A summary and conclusions are given in section 4.

2. Case Synopsis, Model Description, and Experimental Setup

On 21 August 2014, a precipitation event took place over north central Mongolia. The amount of daily accumulated surface precipitation from 00 UTC 21 August to 00 UTC 22 August was 30 mm in Ulaanbaatar, capital of Mongolia, and 19 mm in Darkhan. The two locations are indicated in Figure 1. The daily accumulated surface precipitation amount of ~20–30 mm can be regarded as a special event in Mongolia considering that the average annual precipitation amount in Mongolia is ~210 mm (Dagvadorj et al., 2014).

The synoptic-scale features associated with the precipitation event are analyzed using the ERA-Interim reanalysis data (Dee et al., 2011). Figure 1 shows the mean sea level pressure and 850 hPa temperature fields, and Figure 2 shows the 500 hPa geopotential height and 200 hPa horizontal wind fields. Analysis times are at 12 UTC 20, 00 UTC 21, 12 UTC 21, and 00 UTC 22 August 2014. At 12 UTC 20 August, a cold high is located north of Mongolia and a warm low is located south of Mongolia (Figure 1a). An upper level cold low that is associated with the low-level cold high exists, and the polar jet streams along the border of the upper level cold low (Figure 2a). For the next 12 h, the low-level cold high moves southeastward and the low-level warm low changes little in its position (Figure 1b). The flow of the polar jet is strengthened in the north-south direction (Figure 2b). At 00 UTC 21 August, the 500 hPa geopotential height at the center of the upper level cold low is 5490 m.

The low-level warm low moves northeastward from 00 UTC 21 August to 12 UTC 21 August and is located southeast of Ulaanbaatar at 12 UTC 21 August (Figure 1c). In the meanwhile, the low-level cold high moves southeastward. The gradients of pressure and temperature are enhanced so that a cold front is developed near Darkhan. In the upper layer, the cold low moves eastward and the flow of the polar jet is further strengthened in the north-south direction (Figure 2c). As the cold low and the polar jet move eastward during this period, the entrance of the polar jet is located northwest of Darkhan at 12 UTC 21 August. At this time, the low-level warm low is located on the right side of the entrance of the upper level jet. Accordingly, the vertical motion is strengthened and the low-level warm low is developed: the pressure at the center of the low-level warm low at 12 UTC 21 August is lower compared to the previous time. The minimum mean sea level pressure of the low-level warm low at 12 UTC 21 August is 999 hPa. It is noted that at the cold front the isobars are generally parallel to the isotherms. From 12 UTC 21 August to 00 UTC 22 August, the low-level cold high is further extended southeastward (Figure 1d). At 00 UTC 22 August, the cold front had passed through Darkhan. The low-level warm low moves further northeastward during this period.

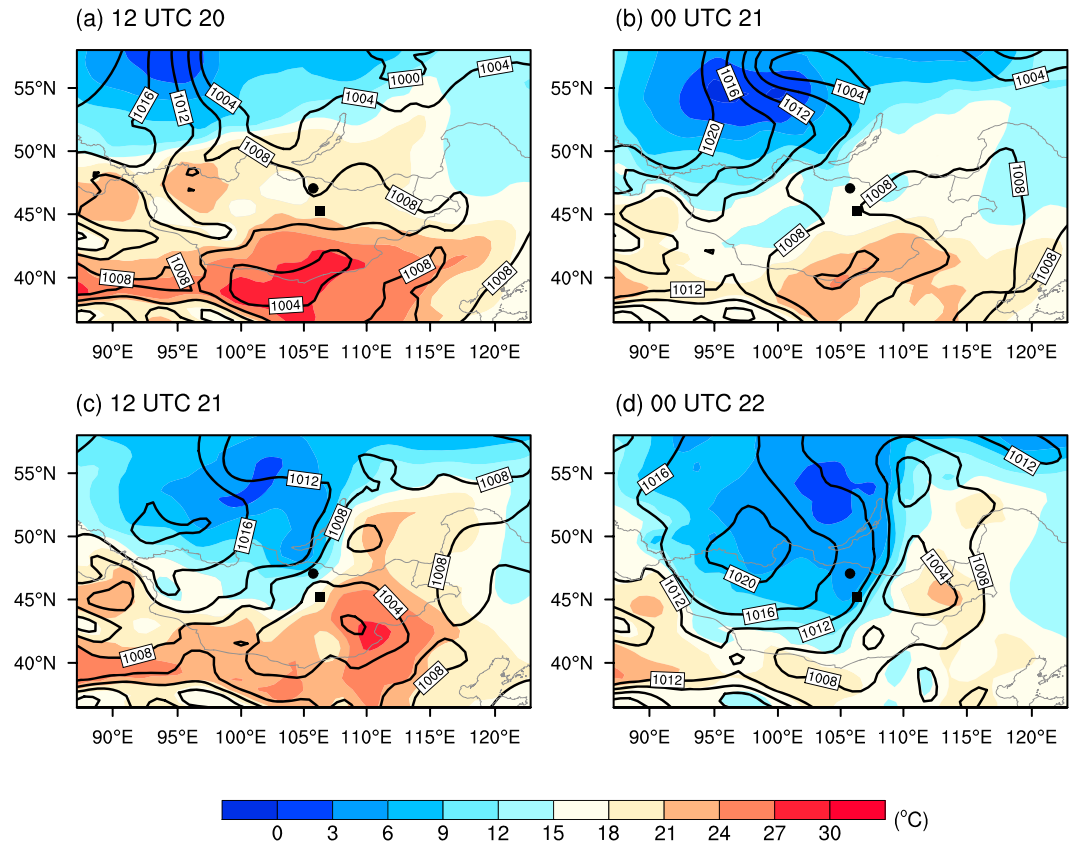


Figure 1. Mean sea level pressure (hPa, black solid lines) and 850 hPa temperature (color shaded) fields at (a) 12 UTC 20, (b) 00 UTC 21, (c) 12 UTC 21, and (d) 00 UTC 22 August 2014 from the ERA-Interim reanalysis data. The locations of Darkhan and Ulaanbaatar observatories are denoted by the small circle and small square in each frame, respectively.

To numerically simulate the precipitation event described above, the Weather Research and Forecasting (WRF) model v3.7.1 (Skamarock et al., 2008) is used. The bin microphysics scheme of the Hebrew University Cloud Model is implemented in the WRF model (Lee & Baik, 2016, 2017). The bin microphysics scheme used in this study considers seven hydrometeor types (liquid drop, three ice crystals (column, plate, and dendrite), snow, graupel, and hail) and aerosol. The bin microphysics scheme uses 43 mass-doubling bins to describe the size distributions of each hydrometeor and aerosol. To consider the gradual melting of large ice particles, the liquid fractions of snow, graupel, and hail are predicted (Phillips et al., 2007). The rimed fraction of snow is also predicted and used to calculate the properties of snow (density and terminal velocity). A simple breakup parameterization of large snow particles (Khain et al., 2011) is incorporated. In the present study, the turbulence-induced collision enhancement is not considered. A more description of the bin microphysics scheme is given in Khain et al. (2011) and Lee and Baik (2016).

Compared to Lee and Baik (2017), the bin microphysics scheme is further improved by considering the IQS model in which the multiple collisions of cloud particles within a time step are allowed (Lkhamjav et al., 2017; Young, 1975). If collisions of cloud particles in the i th and j th bins are considered, the rate of the change of number concentration is given as (e.g., Lkhamjav et al., 2017)

$$\Delta n_i = \Delta n_j = -n_i n_j K_{ij} \Delta t, \quad (1)$$

where n_i and n_j are the number concentrations of cloud particles in the i th and j th bins, respectively; K_{ij} is the collection kernel between the i th and j th bins; and Δt is the time step. The NQS model assumes an infinitesimally small time step within which a cloud particle either collides with other cloud particle once or does not collide. However, since the time step used is not infinitesimally small but finite, a cloud particle can collide with other cloud particle more than one time. When multiple collisions within a finite time step are rigorously considered, the probability of the number of collisions in the IQS model is given as a Poisson distribution form.

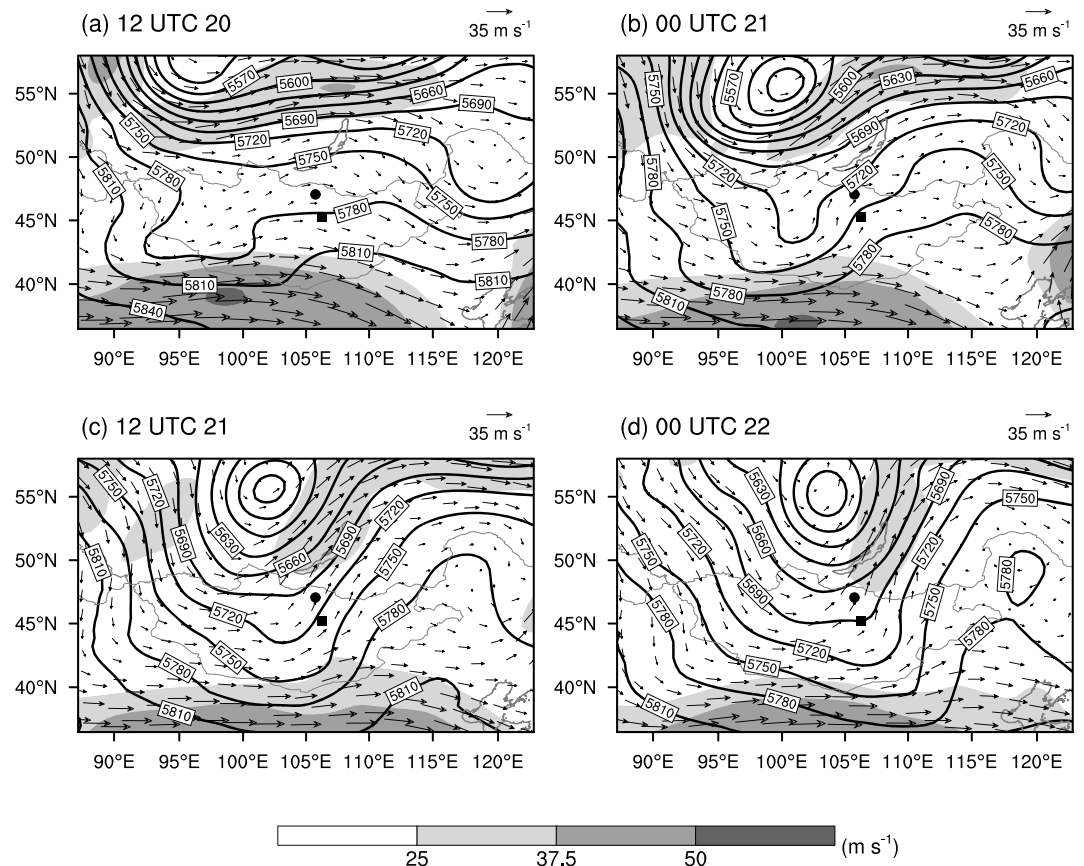


Figure 2. Same as in Figure 1 but for 500 hPa geopotential height (m, black solid lines) and 200 hPa horizontal wind vector and speed (shaded).

$$P(x) = \frac{p^x e^{-p}}{x!}, \quad (2)$$

where x is the number of collisions and p is the average number of collisions [e.g., $p = n_j K_{ij} \Delta t$ for cloud particles in the i th bin in (1)]. In the IQS model, the average number of collisions is the same as that in the NQS model but some cloud particles have a chance to collide with other cloud particle more than one time within a time step. That is, in the NQS model, only $P(0)$ and $P(1)$ are not zero, which are $1 - p$ and p , respectively. On the other hand, in the IQS model, the summation of $P(x)$ from $x = 0$ to ∞ is 1 and the expectation value of x is p , but $P(x)$ with $x \geq 2$ have also certain nonzero values. Note that the Poisson approach in the IQS model is not applied to the collisional breakup process.

Two one-way nested domains are considered (Figure 3). The horizontal grid size is 5 km in the inner domain (domain 2 in Figure 3) and 15 km in the outer domain (domain 1 in Figure 3). The model top is 50 hPa (~ 20 km), and the number of vertical layers is 41. To provide initial and boundary conditions in the outer domain, the ERA-Interim data (Dee et al., 2011) are used. The radiation scheme (Iacono et al., 2008) is used for the parameterization of shortwave and longwave radiation, the Yonsei University scheme (Hong et al., 2006) for the parameterization of the planetary boundary layer, and the Kain-Fritsch scheme (Kain, 2004) for the parameterization of subgrid-scale cumulus convection, which is applied only to the outer domain. The Noah land surface model (Chen & Dudhia, 2001) is used. The initial aerosol number concentration (here initial cloud condensation nucleus (CCN) number concentration at 1% supersaturation) is set to 300 cm^{-3} near the surface, and the size distribution of aerosol is set to follow the Köhler equation (Köhler, 1936) and the Twomey equation (Twomey, 1959). The WRF model is integrated for 36 h starting from 12 UTC 20 August 2014. The time step used is 20 s in the inner domain and 60 s in the outer domain.

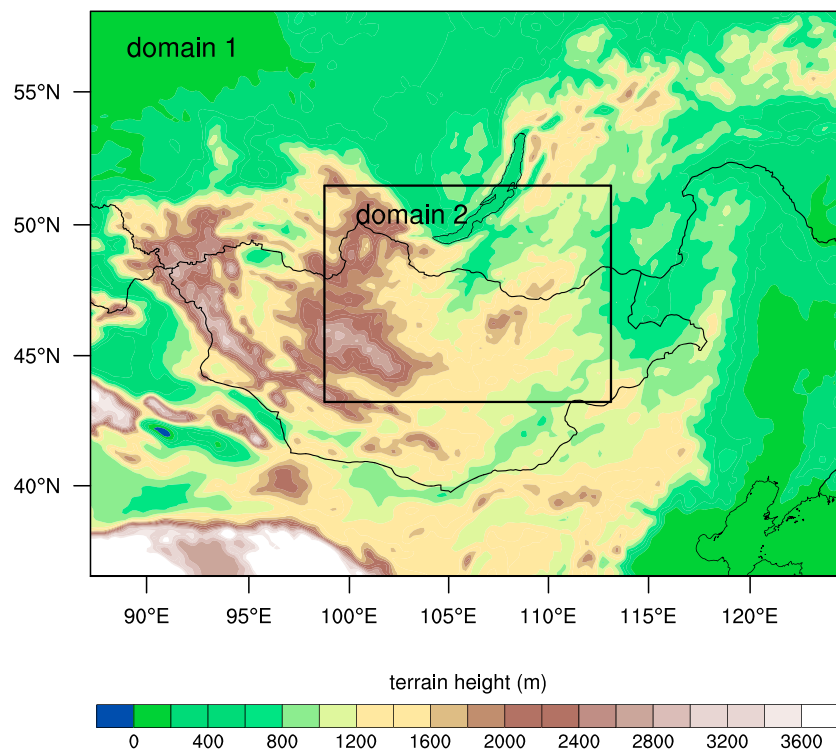


Figure 3. Two nested computational domains and terrain height.

3. Results and Discussion

3.1. Model Validation

Figures 4a–4c show the distributions of the observed and IQS model-simulated surface precipitation amount in the domain from 00 UTC 21 to 00 UTC 22 August 2014. The observation data are from the Integrated Multi-satellite Retrievals for GPM (IMERG), where GPM stands for Global Precipitation Measurement, (Figure 4a) and the National Agency for Meteorology and Environment Monitoring (NAMEM) of Mongolia (Figure 4b). The difference in 24 h accumulated surface precipitation amount between the IQS and NQS models is presented in Figure 4d. The IMERG data set used in this study is version 03D and multisatellite precipitation estimate with gauge calibration (final run) and has a horizontal resolution of 0.1° and a temporal resolution of half an hour (Huffman et al., 2015). Since many parts of the study area are remote mountainous areas, the number of meteorological observatories (32) is not large enough to obtain precipitation distribution fields in high spatial resolution. To compare all the precipitation data at same spatial resolution, an area average over $0.5^\circ \times 0.5^\circ$ is considered (Figure 4). The simulation result (Figure 4c) exhibits a strong precipitation band along the northeast-southwest direction across the center region of the domain including Darkhan, some of this feature being revealed in the rain gauge data. This strong precipitation band is consistent with the direction of the cold front in Figure 1c. Moreover, another relatively strong precipitation is simulated east of Darkhan, which is associated with the low-level warm low ahead of the cold front (see Figures 1b and 1c).

It is seen from Figure 4d that the deviation of the IQS model from the NQS model is to a large extent positive in the domain, particularly at and near Darkhan, although an alternating pattern (i.e., spatial shifts) is seen. Because the IQS (also NQS) model tends to underestimate the 24 h accumulated surface precipitation amount compared to the IMERG data, in this regard, this positive deviation partially alleviates the negative bias of the NQS model. In spite of the uncertainty of the IMERG data and the insufficient spatial coverage of the rain gauge data, it seems that the IQS model improves over the NQS model by taking account of multiple collisions of cloud particles.

It is noted that IMERG data are based upon the combined analysis of intermittent satellite measurements and limited rain gauge measurements. Thus, it may be relatively not good to calculate and discuss bias and error due to large uncertainty in the accumulated surface precipitation amounts, although the temporal and

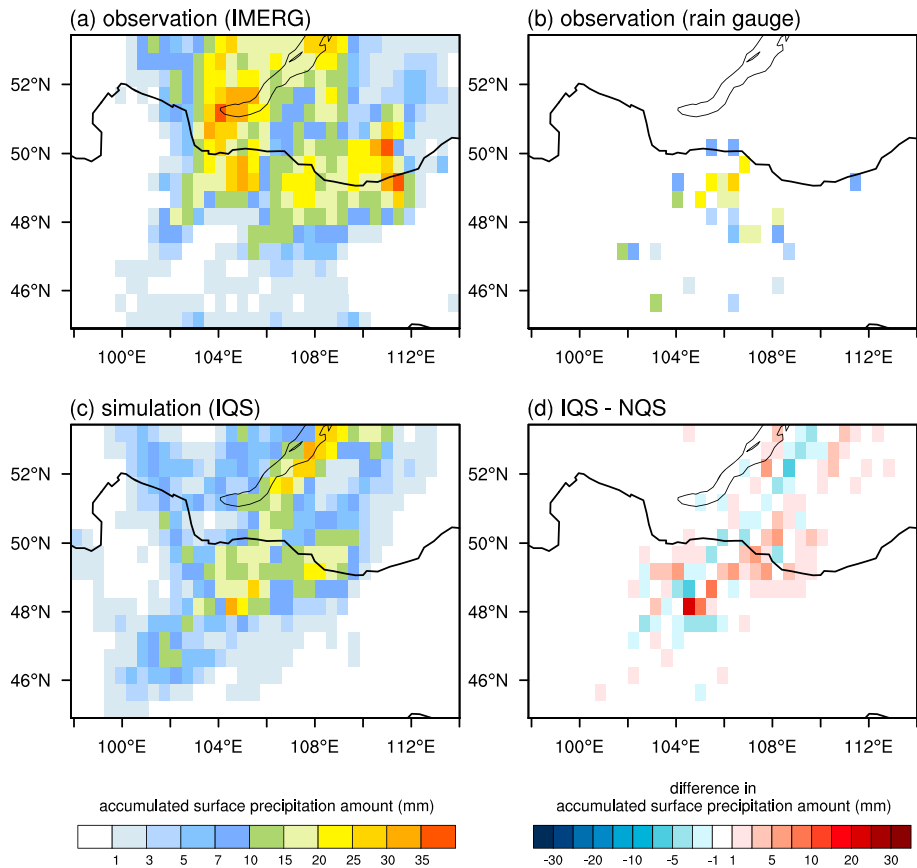


Figure 4. Distributions of accumulated surface precipitation amount from 00 UTC 21 to 00 UTC 22 August 2014: (a) Integrated Multi-satellite Retrievals for GPM (IMERG) data, (b) rain gauge data from the National Agency for Meteorology and Environment Monitoring (NAMEM) of Mongolia, and (c) the IQS model simulation. (d) Difference in accumulated surface precipitation amount between the IQS model and the NQS model. Note that Figure 4b is constructed using rain gauge data at 32 meteorological observatories. In Figure 4b, the areas with white color stand for no precipitation, 24 h accumulated surface precipitation amount smaller than 1 mm, or the absence of observation.

spatial patterns of surface precipitation are relatively good to be discussed. Keeping this in mind, the root-mean-square error of 24 h accumulated surface precipitation amount is calculated using the simulation data of the IQS and NQS models and the rain gauge data. The simulation data are bi-linearly interpolated to the locations of meteorological observatories. The root-mean-square error is 9.2 mm in the IQS model and 10.2 mm in the NQS model, showing an improvement of the IQS model over the NQS model. Also, the deviation of simulated 24 h accumulated surface precipitation amount from the rain gauge data is calculated. The mean deviation is -6.0 mm in the IQS model and -6.5 mm in the NQS model, indicating that both the models underestimate 24 h accumulated surface precipitation amount, but the prediction performance is better in the IQS model than in the NQS model.

Two additional simulations are conducted to examine the impacts of different initial conditions on precipitation prediction for the case considered in this study. For this, following Lee and Baik (2016), the initial potential temperature at every grid point is perturbed by the random noise uniformly distributed between -0.3 K and 0.3 K in the IQS and NQS model simulations. Except for the initial potential temperature perturbations, the experimental setup is the same as that described in section 2. Using the simulation and rain gauge data, the root-mean-square error and deviation are calculated. The root-mean-square error of 24 h accumulated surface precipitation amount is 9.5 mm in the IQS model and 9.7 mm in the NQS model. Thus, the IQS model improves over the NQS model, which is also found in the IQS and NQS model simulations without the initial potential temperature perturbations. The mean deviation of simulated 24 h accumulated surface precipitation amount is -5.3 mm in the IQS model and -6.1 mm in the NQS model. This means that the 24 h

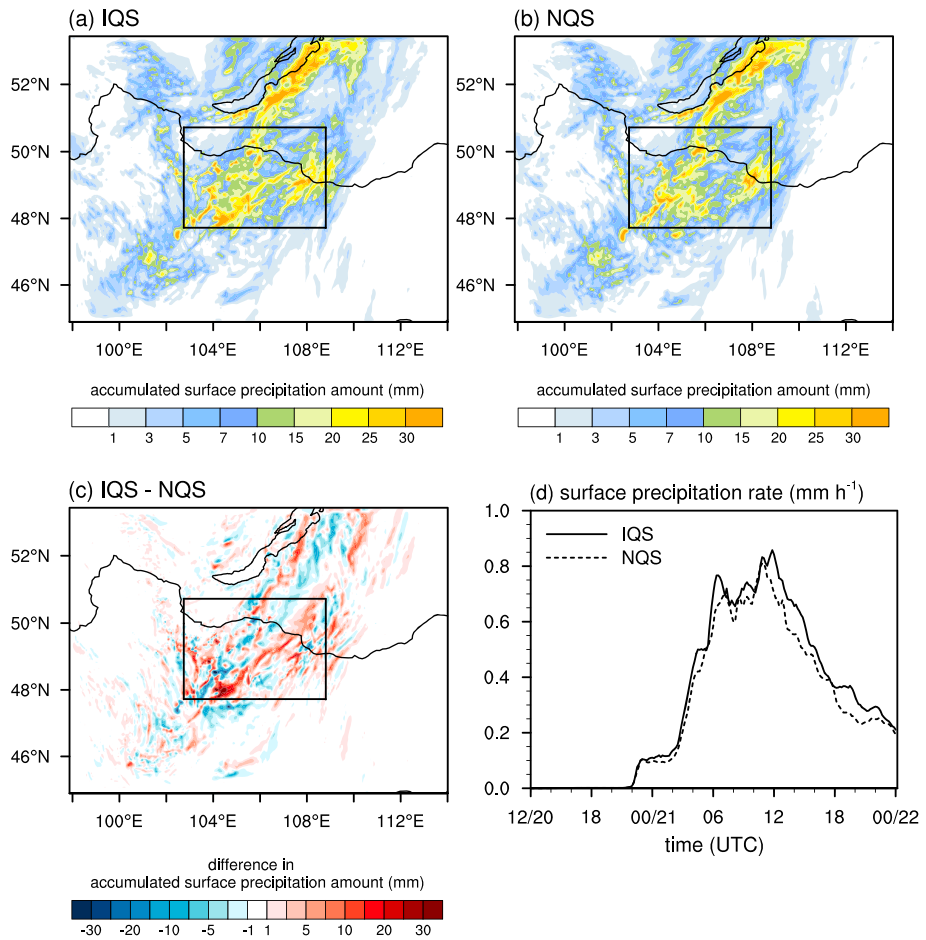


Figure 5. Distributions of accumulated surface precipitation amount from 00 UTC 21 to 00 UTC 22 August 2014 in (a) the IQS model and (b) the NQS model. (c) Difference in accumulated surface precipitation amount between the IQS model and the NQS model. (d) Time series of surface precipitation rate in the IQS and NQS models. In Figure 5d, the surface precipitation rate is averaged over the analysis area centered at Darkhan observatory (marked as the rectangle).

accumulated surface precipitation amount is underestimated in both the models, but the IQS model is better than the NQS model in the performance of precipitation prediction, which is also found in the IQS and NQS model simulations without the initial potential temperature perturbations.

3.2. Impacts of the IQS Model on Precipitation and Cloud Microphysics

Figures 5a–5c show the distributions of 24 h accumulated surface precipitation amount in the IQS and NQS models and the difference between them. The accumulated surface precipitation amount in the domain is larger in the IQS model than in the NQS model. Focusing on a region of north central Mongolia where the surface precipitation amount is large (marked as the rectangle in Figure 5, hereafter called the analysis area), the increase in surface precipitation amount in the IQS model is overall more pronounced in the analysis area than in its outside area. The time series of surface precipitation rate averaged over the analysis area in the IQS and NQS models are presented in Figure 5d. The surface precipitation rate is consistently larger throughout the simulation period in the IQS model than in the NQS model despite spatial shifts in the distribution of surface precipitation. The 24 h accumulated surface precipitation amount averaged over the analysis area is 11.7 mm in the IQS model and 10.5 mm in the NQS model, 11.4% larger in the IQS model relative to the NQS model.

We have analyzed the distributions of accumulated surface precipitation amount in the IQS and NQS model simulations with the initial potential temperature perturbations. It is found that the spatial patterns of accumulated surface precipitation amount are similar to those in the IQS and NQS model simulations

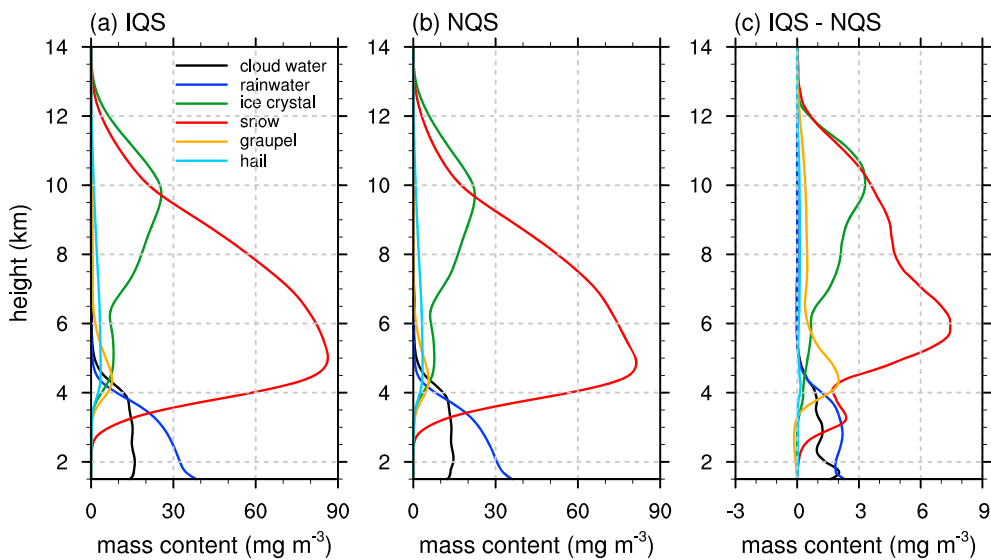


Figure 6. Vertical profiles of hydrometeor mass contents averaged over 10–20 UTC 21 August 2014 and the analysis area in (a) the IQS model and (b) the NQS model. (c) Differences in hydrometeor mass contents between the IQS model and the NQS model.

without the initial potential temperature perturbations. The time series of surface precipitation rate averaged over the analysis area show that before \sim 15 UTC the surface precipitation rate is larger in the IQS model than in the NQS model and after \sim 15 UTC the surface precipitation rate is smaller in the IQS model than in the NQS model. The 24 h accumulated surface precipitation amount averaged over the analysis area is larger in the IQS model (11.4 mm) than in the NQS model (10.9 mm), 4.6% larger in the IQS model relative to the NQS model. These results indicate some sensitivity of precipitation prediction to initial conditions. In spite of the sensitivity, the IQS model produces more precipitation than the NQS model in both the experimental settings (with and without the initial potential temperature perturbations). Further in-depth studies are needed to better understand the impacts of different initial conditions on precipitation prediction in the framework of the IQS and NQS models using an ensemble approach and many precipitation cases.

Figures 6a and 6b show the vertical profiles of hydrometeor mass contents averaged over 10–20 UTC 21 August 2014 and the analysis area in the IQS and NQS models. Note that the ice crystal mass content is the sum of column-, plate-, and dendrite-type ice crystal mass contents. In both the IQS and NQS models, the snow mass content is dominant, the averaged freezing level is \sim 4 km, and snow particles are simulated even below the freezing level because of the gradual melting of snow particles. Also, in both the models, supercooled drops exist largely between the freezing level and $z \sim$ 5 km.

The differences in hydrometeor mass contents between the IQS and NQS models (Figure 6c) show that the mass contents of cloud water, rainwater, ice crystal, snow, and graupel increase in the IQS model relative to the NQS model and the hail mass content is almost the same in both the models. Among the increases in the hydrometeor mass contents, the increase in snow mass content is the most noticeable. The maximum increase in snow mass content is 7.4 mg m^{-3} at $z = 5.9 \text{ km}$. The increase in ice crystal mass content above the freezing level is also noticeable, and its maximum increase is 3.3 mg m^{-3} at $z = 10.1 \text{ km}$. The increase in graupel mass content is large between $z \sim 4 \text{ km}$ and $z \sim 6 \text{ km}$. The maximum increase in graupel mass content is 2.0 mg m^{-3} at $z = 4.4 \text{ km}$. The mass contents of cloud water and rainwater increase noticeably below $z \sim 4 \text{ km}$. The enhanced large drop formation due to multiple collisions of cloud particles in the IQS model results in an increase in rainwater mass content. In addition to the enhanced large drop formation, the increased mass contents of snow and graupel in the IQS model can have a significant role in controlling rainwater mass content through melting.

The vertical profiles of vertical velocity and net heating rate due to cloud microphysical processes in the IQS and NQS models are presented in Figure 7. The vertical velocity and net heating rate are averaged over 10–20

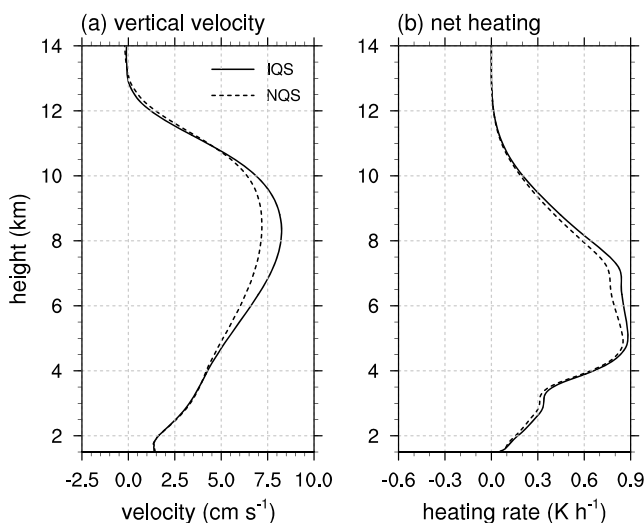


Figure 7. Vertical profiles of (a) vertical velocity and (b) net heating rate due to cloud microphysical processes averaged over 10–20 UTC 21 August 2014 and the analysis area in the IQS model and the NQS model.

vertical velocity shows that the upward motion is stronger after ~12 UTC in the IQS model than in the NQS model (figure not shown). The difference in ice crystal mass content is large after ~12 UTC, and the difference in snow mass content is large after ~14 UTC. This implies that the increase in snow mass content in the IQS model is mainly caused by the increase in ice crystal mass content. The increase in snow mass content propagates downward, and it induces an increase in rainwater mass content through melting, hence resulting in the enhanced surface precipitation amount. Note that the significant increase in rainwater mass content before ~14 UTC is due to multiple collisions of cloud particles in the IQS model. Before ~12 UTC, the mass contents of ice crystal and snow are smaller in the IQS model than in the NQS model. This implies that in the IQS model, ice-phased microphysical processes before ~12 UTC are less active than those after ~12 UTC.

Figure 9 shows the time-height sections of horizontally averaged deposition, condensation, riming, and melting rates in the IQS model and the differences in the rates between the IQS and NQS models. The increases in deposition and condensation in the IQS model are clear, and their trends are similar to those of the increases in snow and raindrop in the IQS model. This implies that the increases in snow and drop mass contents in the IQS model are largely due to the increased deposition and condensation, respectively. Also, these increases in snow and drop mass contents again contribute to the increases in deposition and condensation, respectively, which intensifies the differences in snow and drop mass contents. Rimming just above the freezing level is stronger in the IQS model than in the NQS model. The increase in ice mass content due to riming after ~14 UTC in the IQS model is mainly caused by the riming of snow (Figures 8d and 9f). On the other hand, the increase in ice mass content due to riming before ~14 UTC in the IQS model is mainly caused by the riming of graupel (Figures 8f and 9f). Rimming plays a role in increasing snow mass content after ~14 UTC in the IQS model, and the increased snow mass content results in the enhanced surface precipitation amount through melting (Figure 9h). Although the graupel mass content is also increased before ~14 UTC in the IQS model, reduced ice-phased microphysical processes appear to result in the decreased melting of ice particles. The overall enhancement of deposition, condensation, and riming causes more latent heat release in the IQS model than in the NQS model (Figure 7b), which contributes to the stronger upward motion in the IQS model than in the NQS model (Figure 7a).

The vertical profiles of the vertical fluxes of cloud water and ice crystal in the IQS and NQS models averaged over 10–20 UTC 21 August 2014 and the analysis area are presented in Figure 10. Here the vertical flux of any hydrometeor is defined as the hydrometeor mass content times ($w + v_t$), where w is the vertical velocity and v_t is the terminal velocity of the hydrometeor (v_t is negative). In both the IQS and NQS models, the vertical flux of cloud water is positive; that is, cloud droplets are transported upward. Between $z \sim 1.5$ km and $z \sim 5.5$ km, the vertical flux of cloud water is larger in the IQS model than in the NQS model. The vertical flux of ice crystal

UTC 21 August 2014 and the analysis area. The vertical profiles of vertical velocity in the IQS and NQS models are overall similar to each other, but there is a difference. In the mid-to-upper troposphere, the upward motion is stronger in the IQS model than in the NQS model. The vertical profiles of the net heating rate due to cloud microphysical processes in the IQS and NQS models are also overall similar to each other, which are also positive in the mid-to-upper troposphere. The positive heating rate is consistently larger in the IQS model than in the NQS model. Figure 7 indicates that the increase in heating due to microphysical processes in the IQS model induces stronger upward motion which in turn enhances microphysical processes, thus promoting interactions of cloud microphysics with dynamics.

Figure 8 shows the time-height sections of horizontally averaged ice crystal, snow, graupel, and rainwater mass contents in the IQS model and the differences in ice crystal, snow, graupel, and rainwater mass contents between the IQS and NQS models. The ice crystal, snow, and graupel mass contents are large before ~12 UTC, and they exhibit a decreasing trend after ~12 UTC (Figures 8a, 8c, and 8e). The differences in ice crystal and snow mass contents are consistently positive after ~12 UTC. The analysis of the time-height section of horizontally averaged

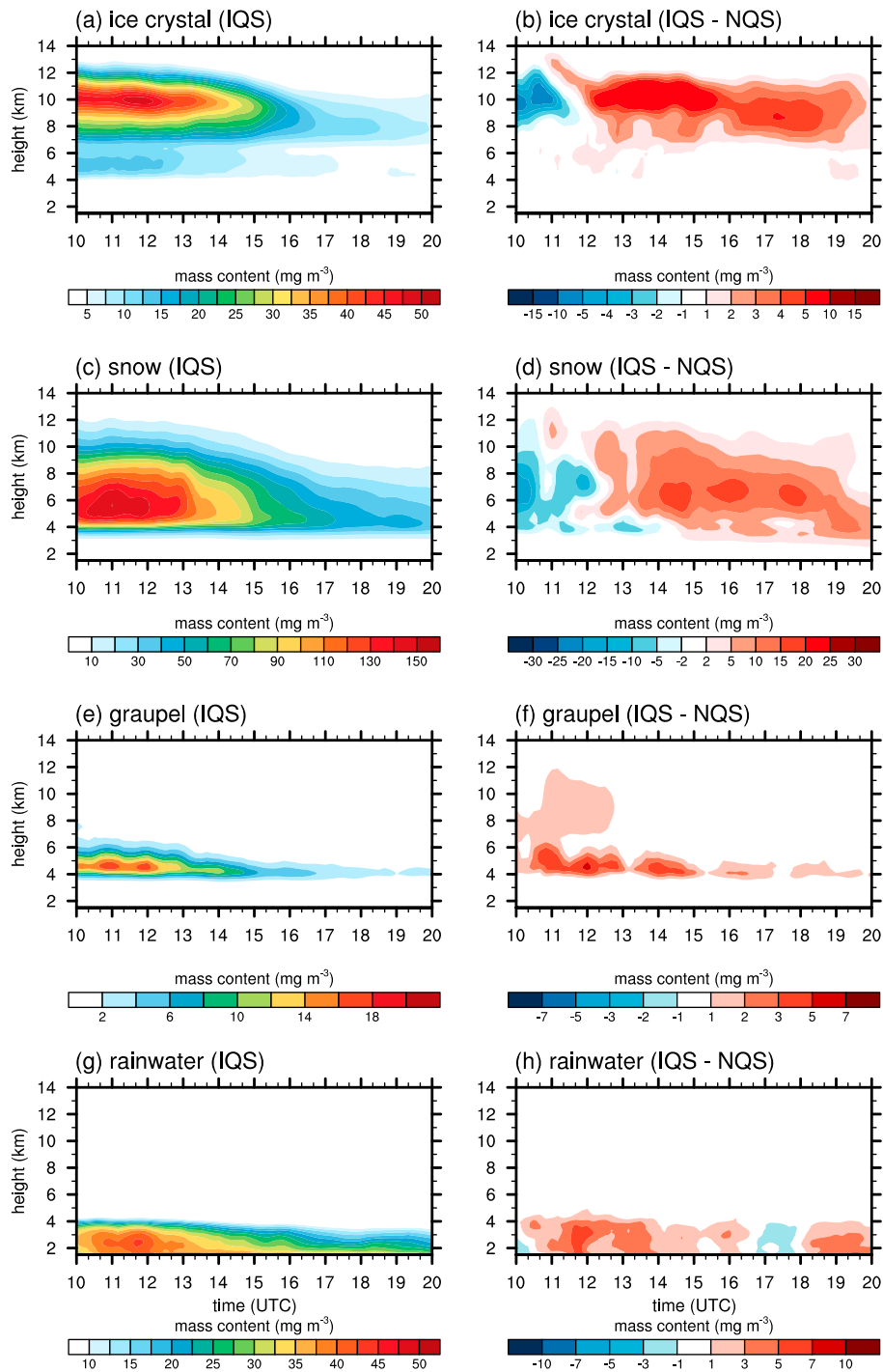


Figure 8. Time-height sections of horizontally averaged (a) ice crystal mass content, (c) snow mass content, (e) graupel mass content, and (g) rainwater mass content in the IQS model. Differences in (b) ice crystal mass content, (d) snow mass content, (f) graupel mass content, and (h) rainwater mass content between the IQS model and the NQS model.

is positive at almost all levels. Some large differences in the vertical flux of ice crystal between the IQS and NQS models are present in the layer between $z \sim 5$ km and $z \sim 11$ km where more vertical transport of ice crystal occurs in the IQS model. As mentioned before, the upward motion is enhanced due to the increased latent heat release in the IQS model, which contributes to the positive differences in the vertical fluxes of cloud water and ice crystal (Figure 10).

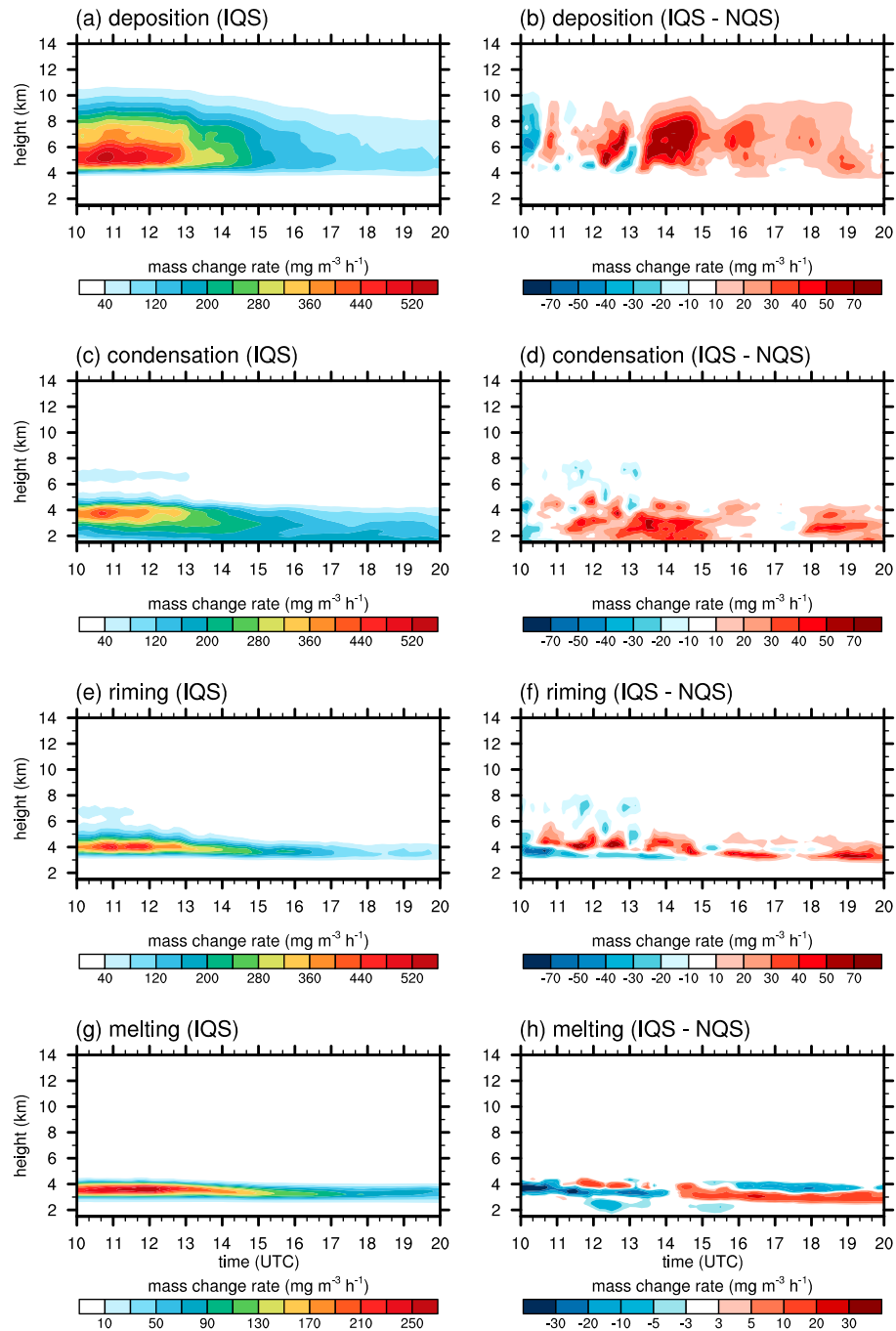


Figure 9. Time-height sections of horizontally averaged (a) deposition rate, (c) condensation rate, (e) riming rate, and (g) melting rate in the IQS model. Differences in (b) deposition rate, (d) condensation rate, (f) riming rate, and (h) melting rate between the IQS model and the NQS model.

Figure 11 shows the size distributions of drop (cloud droplet plus raindrop), snow, and graupel averaged over the 10 h period and the analysis area in the IQS and NQS models and the differences in the size distributions of drop, snow, and graupel between the IQS and NQS models. The size distribution is calculated at $z = 3$ km for drop, at $z = 5$ km for snow, and $z = 4$ km for graupel. In both the IQS and NQS models, the drop size distribution exhibits primary peaks at $\sim 20 \mu\text{m}$ and $\sim 410 \mu\text{m}$ in radius, which belong to cloud droplets and raindrops, respectively. The difference in drop size distribution shows that the drop mass content is increased in the IQS model both in the small drop range (maximum at $\sim 20 \mu\text{m}$) and in the large drop

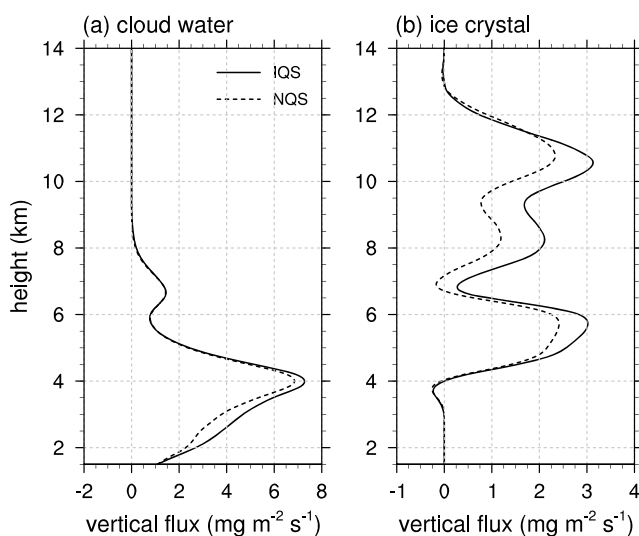


Figure 10. Vertical profiles of the vertical fluxes of (a) cloud water and (b) ice crystal averaged over 10–20 UTC 21 August 2014 and the analysis area in the IQS model and the NQS model.

range (maximum at ~1 mm). The increased large drop mass content contributes to the enhanced surface precipitation amount. It is noted that the drop mass content in a part of medium sizes is decreased in the IQS model. The increased drop mass content in the small drop range in the IQS model results from the difference between the IQS and NQS models. However, unlike in the box model and idealized two-dimensional simulations (Lkhamjav et al., 2017), in the real-case simulation (the present study), it seems to be very difficult to find detailed reasons for the increased drop mass content in the small drop range because of the increased complexity. More activation of CCN due to the increase in upward motion can be a reason. Further study is needed to find reasons for that, in views of microphysics and dynamics feedback.

For the snow size distribution, both the IQS and NQS models share common features that it exhibits a primary peak at ~6 mm in radius and the mass of snow is largely occupied by large snow particles (~0.1–1 cm in radius) (Figure 10c). The difference between the IQS and NQS models is mainly positive; that is, the snow mass content is larger in the IQS model than in the NQS model. In Figure 8, it is shown that the increase in snow mass content is largely caused by the increase in ice crystal mass content. Therefore, it can be deduced that the increase in the mass content of cloud droplets (Figure 11b) causes the increase in ice crystal mass content by

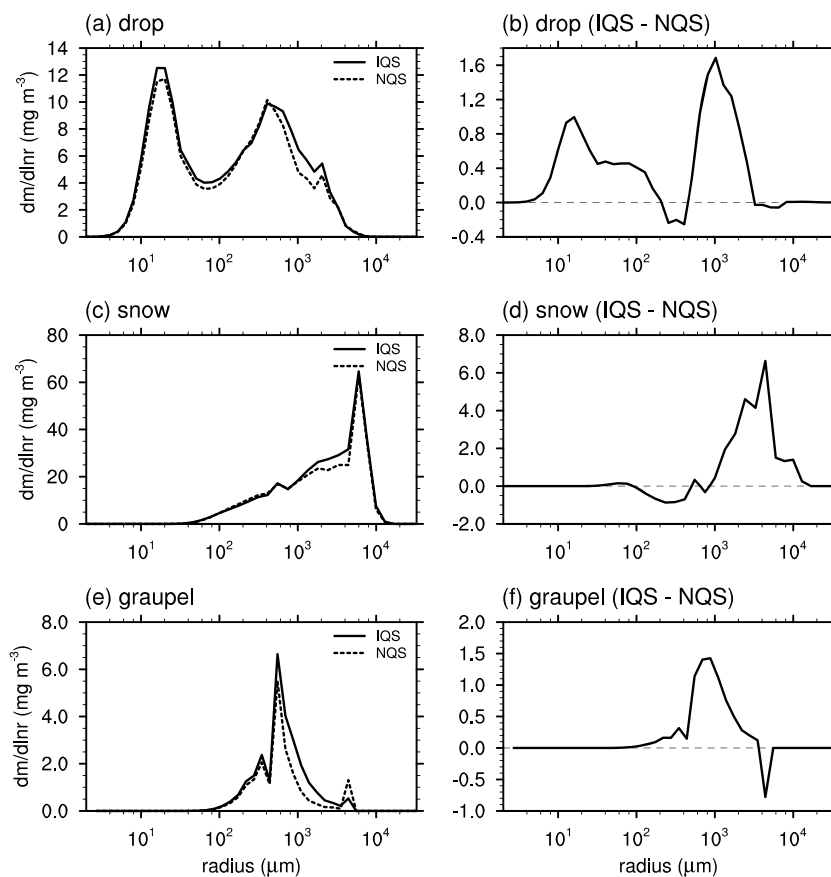


Figure 11. Size distributions of (a) drop at $z = 3$ km, (c) snow at $z = 5$ km, and (e) graupel at $z = 4$ km averaged over 10–20 UTC 21 August 2014 and the analysis area in the IQS and NQS models. Differences in the size distributions of (b) drop, (d) snow, and (f) graupel between the IQS model and the NQS model.

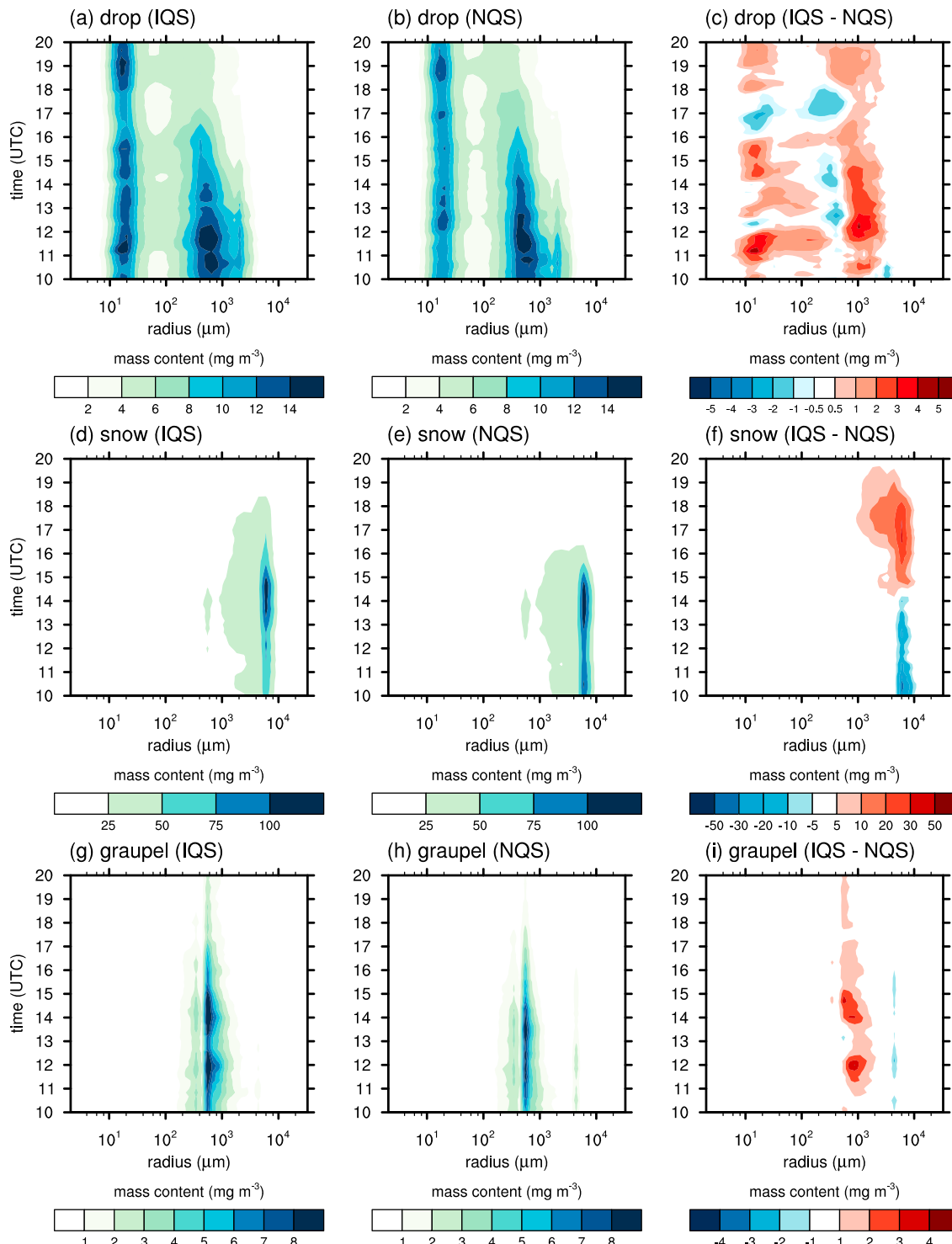


Figure 12. Time evolution of the horizontally averaged size distributions of (a) drop in the IQS model, (b) drop in the NQS model, and (c) difference in drop size distribution between the IQS model and the NQS model. (d–f) Same as Figures 12a–12c, respectively, but for snow. (g–i) Same as Figures 12a–12c, respectively, but for graupel.

increased upward transport of cloud droplets (Figure 10a) and freezing, hence increasing snow mass content. In addition, this increased snow mass content contributes to the increased raindrop mass content (Figures 11b and 11d) through melting, which enhances the surface precipitation amount. The graupel size distribution exhibits a primary peak at ~550 μm in both the IQS and NQS models (Figure 11e). The graupel

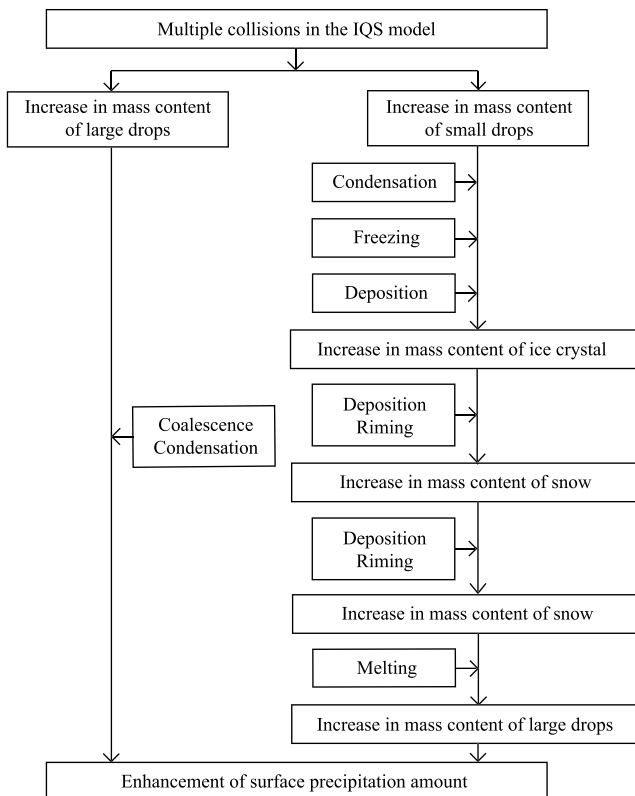


Figure 13. Schematic diagram of microphysical processes that result in the larger surface precipitation amount in the IQS model.

in surface precipitation amount. This pathway is depicted on the left side of the schematic diagram. The increased small drops due to multiple collisions are transported upward, grow through condensation, and then freeze, forming ice crystals. The ice crystals grow by deposition, further increasing ice crystal mass content. The increase in the mass content of ice crystal gives rise to the increase in the mass content of snow through deposition and riming. The mass content of snow is further increased through deposition and riming. The increased mass content of snow increases the mass content of large drops through the melting of snow particles. Thus, the increased mass content of large drops also contributes to the increase in surface precipitation amount. This pathway is depicted on the right side of the schematic diagram.

It should be noted that the schematic diagram shows major microphysics pathways only that lead to the larger amount of surface precipitation in the IQS model. The interactions of microphysics with dynamics in the precipitation systems simulated in this study, which need further investigation, are too complicated to understand fully and be included appropriately in a schematic diagram. The schematic diagram presented, nonetheless, could be a valuable one showing the connections of microphysical processes.

4. Summary and Conclusions

The improved quasi-stochastic model (IQS model) that allows for multiple collisions of cloud particles within a time step was evaluated through precipitation prediction. For this purpose, a precipitation event observed over north central Mongolia on 21 August 2014 was simulated using the Weather Research and Forecasting model with a detailed bin microphysics scheme and the simulation results from the IQS model were compared to those from the normal quasi-stochastic model (NQS model) in which a cloud particle can collide with other cloud particle only once within a time step.

The simulated surface precipitation amount in the IQS model is closer to the observation than that in the NQS model, although both the IQS and NQS models underestimate the surface precipitation amount. It was found that the surface precipitation amount is larger in the IQS model than in the NQS model, particularly over the

mass content is noticeably larger in the IQS model than in the NQS model in the ~0.5–2 mm radius range, with its maximum difference at ~880 μm (Figure 11f).

Figure 12 is the same as Figure 11 but as a form of the time evolution of the size distributions of drop, snow, and graupel and the differences. Figure 12 exhibits the characteristics of the size distributions in more detail. The increases in the mass of small and large drops are seen throughout almost the entire period and are more distinct before ~15 UTC. The increase in the mass of large snow particles is simulated after ~14 UTC (see also Figure 8d). This implies that the increase in the mass of large drops after ~14 UTC is caused by the increase in the mass of large snow particles. The increase in graupel mass content in the ~0.5–2 mm radius range is seen throughout the time period, especially before ~15 UTC. Before ~15 UTC, the riming of snow with increased large drops may result in an increase in graupel mass content. However, Figures 12f and 12i show that after ~15 UTC the contribution of the increased graupel mass content to surface precipitation amount through melting is less significant than the contribution of the increased snow mass content to surface precipitation amount through melting. This results in the decrease in melting before ~14 UTC in the IQS model (Figure 9 h).

Based upon the analysis results of Figures 5–12, we construct a schematic diagram that depicts major pathways of microphysics that result in the larger surface precipitation amount in the IQS model relative to the NQS model (Figure 13). The IQS model that takes account of multiple collisions of cloud particles increases the mass contents of both large drops and small drops. The increased large drops grow through coalescence and condensation, which further increases the mass content of larger drops. The increased mass content of larger drops contributes to the increase

strong precipitation region. Microphysical processes that lead to the larger surface precipitation amount in the IQS model were analyzed in detail. In the IQS model, the mass contents of both large drops and small drops are increased due to multiple collisions of cloud particles. The increased large drops act to increase surface precipitation amount. The increased small drops increase snow mass content through freezing, deposition, and riming. The increased snow mass content also acts to increase surface precipitation amount through melting.

The number of studies that utilize numerical models that include bin microphysics schemes to understand clouds and precipitation has increased in recent years with advances in computing power. The quasi-stochastic collection model that takes account of multiple collisions of cloud particles can be easily implemented in models with bin microphysics schemes, expecting to better simulate cloud and precipitation processes, as demonstrated in this study. This study considered only one precipitation event. Many precipitation events are required to examine the impacts of the IQS model on cloud and precipitation processes, which could vary with environmental conditions, deserving an investigation. Lkhamjav et al. (2017) indicated that the effects of aerosols on the evolution of drop size distribution can be modulated by the IQS model. Aerosol effects on clouds and precipitation in the IQS model through real-case simulations need to be also investigated to better understand cloud-aerosol-precipitation interactions.

Acknowledgments

The authors are grateful to three anonymous reviewers for providing valuable comments on this study. The ERA-Interim reanalysis data are available at <https://www.ecmwf.int/en/research/climate-reanalysis/era-interim>. The IMERG data are available at https://data.nasa.gov/Earth-Science/GPM-Level-3-IMERG-Monthly-0-1-x-0-1-degree-V03/btqh-p7bi?category=Earth-Science&view_name=GPM-Level-3-IMERG-Monthly-0-1-x-0-1-degree-V03. The authors were supported by the Korea Meteorological Administration Research and Development Program under grants KMIPA 2015-5100 and KMIPA 2015-5190. The authors thank supercomputer management division of the Korea Meteorological Administration for providing us with the supercomputer resource.

References

- Berry, E. X. (1967). Cloud droplet growth by collection. *Journal of the Atmospheric Sciences*, 24, 688–701.
- Chen, F., & Dudhia, J. (2001). Coupling an advanced land-surface/hydrology model with the Penn State/NCAR MM5 modeling system. Part I: Model description and implementation. *Monthly Weather Review*, 129, 569–585.
- Dagvadorj, D., Batjargal, Z., & Natsagdorj, L. (2014). MARCC 2014: Mongolia Second Assessment Report on Climate Change 2014, Ministry of Environment and Green Development of Mongolia, Mongolia.
- Dee, D. P., Uppala, S. M., Simmons, A. J., Berrisford, P., Poli, P., Kobayashi, S., ... Vitart, F. (2011). The ERA-Interim reanalysis: Configuration and performance of the data assimilation system. *Quarterly Journal of the Royal Meteorological Society*, 137(656), 553–597. <https://doi.org/10.1002/qj.828>
- Gillespie, D. T. (1972). The stochastic coalescence model for cloud droplet growth. *Journal of the Atmospheric Sciences*, 29, 1496–1510.
- Hong, S.-Y., Noh, Y., & Dudhia, J. (2006). A new vertical diffusion package with an explicit treatment of entrainment processes. *Monthly Weather Review*, 134, 2318–2341.
- Houze, R. A. Jr. (2014). *Cloud dynamics*. United States: Academic Press.
- Huffman, G., Bolvin, D. T., & Nelkin, E. J. (2015). Integrated Multi-satellite Retrievals for GPM (IMERG) technical documentation, NASA Goddard Space Flight Center, 19 June. Retrieved from http://pmmm.nasa.gov/sites/default/files/document_files/IMERG_doc.pdf
- Iacono, M. J., Delamere, J. S., Mlawer, E. J., Shephard, M. W., Clough, S. A., & Collins, W. D. (2008). Radiative forcing by long-lived greenhouse gases: Calculations with the AER radiative transfer models. *Journal of Geophysical Research*, 113, D13103. <https://doi.org/10.1029/2008JD009944>
- Iguchi, T., Nakajima, T., Khain, A. P., Saito, K., Takemura, T., Okamoto, H., ... Tao, W.-K. (2012). Evaluation of cloud microphysics in JMA-NHM simulations using bin or bulk microphysical schemes through comparison with cloud radar observations. *Journal of the Atmospheric Sciences*, 69, 2566–2586.
- Kain, J. S. (2004). The Kain-Fritsch convective parameterization: An update. *Journal of Applied Meteorology*, 43, 170–181.
- Kessler, E. (1969). On the distribution and continuity of water substance in atmospheric circulations. MA: AMS.
- Khain, A., Beheng, K., Heymsfield, A., Korolev, A., Krichak, S., Levin, Z., ... Yano, J.-I. (2015). Representation of microphysical processes in cloud-resolving models: Spectral (bin) microphysics versus bulk parameterization. *Reviews of Geophysics*, 53, 247–322. <https://doi.org/10.1002/2014RG000468>
- Khain, A., Rosenfeld, D., Pokrovsky, A., Blahak, U., & Ryzhkov, A. (2011). The role of CCN in precipitation and hail in a mid-latitude storm as seen in simulations using a spectral (bin) microphysics model in a 2D dynamic frame. *Atmospheric Research*, 99, 129–146.
- Khain, A., Sednev, I., & Khvorostyanov, V. (1996). Simulation of coastal circulation in the eastern Mediterranean using a spectral microphysics cloud ensemble model. *Journal of Climate*, 9, 3298–3316.
- Köhler, H. (1936). The nucleus in and the growth of hygroscopic droplets. *Journal of the Chemical Society, Faraday Transactions*, 32, 1152–1161.
- Lee, H., & Baik, J.-J. (2016). Effects of turbulence-induced collision enhancement on heavy precipitation: The 21 September 2010 case over the Korean Peninsula. *Journal of Geophysical Research: Atmospheres*, 121, 12,319–12,342. <https://doi.org/10.1002/2016JD025168>
- Lee, H., & Baik, J.-J. (2017). A physically based autoconversion parameterization. *Journal of the Atmospheric Sciences*, 74, 1599–1616.
- Lin, K.-S. S., & Hong, S.-Y. (2010). Development of an effective double-moment cloud microphysics scheme with prognostic cloud condensation nuclei (CCN) for weather and climate models. *Monthly Weather Review*, 138, 1587–1612.
- Lin, Y.-L., Farly, R. D., & Orville, H. D. (1983). Bulk parameterization of the snow field in a cloud model. *Journal of Climate and Applied Meteorology*, 22, 1065–1092.
- Lkhamjav, J., Lee, H., Jeon, Y.-L., & Baik, J.-J. (2017). Examination of an improved quasi-stochastic model for the collisional growth of drops. *Journal of Geophysical Research: Atmospheres*, 122, 1713–1724. <https://doi.org/10.1002/2016JD025904>
- Lynn, B. H., Khain, A. P., Dudhia, J., Rosenfeld, D., Pokrovsky, A., & Seifert, A. (2005a). Spectral (bin) microphysics coupled with a mesoscale model (MM5). Part I: Model description and first results. *Monthly Weather Review*, 133, 44–58.
- Lynn, B. H., Khain, A. P., Dudhia, J., Rosenfeld, D., Pokrovsky, A., & Seifert, A. (2005b). Spectral (bin) microphysics coupled with a mesoscale model (MM5). Part II: Simulation of a CaPE rain event with a squall line. *Monthly Weather Review*, 133, 59–71.
- Phillips, V. T. J., Pokrovsky, A., & Khain, A. (2007). The influence of time-dependent melting on the dynamics and precipitation production in maritime and continental storm clouds. *Journal of the Atmospheric Sciences*, 64, 338–359.
- Pruppacher, H. R., & Klett, J. D. (1997). *Microphysics of clouds and precipitation*. Netherlands: Kluwer Academic.

- Sato, Y., Nakajima, T., Suzuki, K., & Iguchi, T. (2009). Application of a Monte Carlo integration method to collision and coagulation growth processes of hydrometeors in a bin-type model. *Journal of Geophysical Research*, 114, D09215. <https://doi.org/10.1029/2008JD011247>
- Seifert, A., & Beheng, K. (2006). A two-moment cloud microphysics parameterization for mixed-phase clouds. Part 1: Model description. *Meteorology and Atmospheric Physics*, 92, 45–66.
- Skamarock, W. C., Klemp, J. B., Dudhia, J., Gill, D. O., Barker, D. M., Duda, M. G., ... Powers, J. G. (2008). A description of the Advanced Research WRF version 3 (NCAR Tech. Note NCAR/TN-475 + STR, 113 pp.).
- Telford, J. (1955). A new aspect of coalescence theory. *Journal of Meteorology*, 12, 436–444.
- Twomey, S. (1959). The nuclei of natural cloud formation. Part II: The supersaturation in natural clouds and the variation of cloud droplet concentration. *Pure and Applied Geophysics*, 43, 243–249.
- Young, K. C. (1975). The evolution of drop spectra due to condensation, coalescence and breakup. *Journal of the Atmospheric Sciences*, 32, 965–973.